

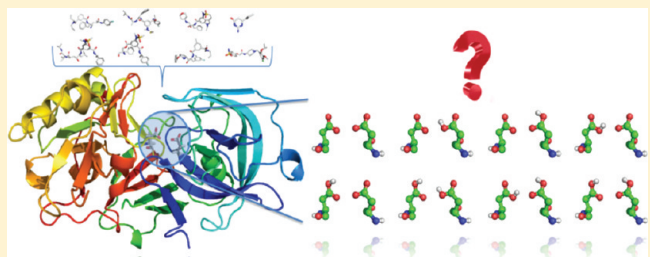
Protonation States of the Catalytic Dyad of β -Secretase (BACE1) in the Presence of Chemically Diverse Inhibitors: A Molecular Docking Study

Arghya Barman and Rajeev Prabhakar*

Department of Chemistry, University of Miami, 1301 Memorial Drive, Coral Gables, Florida 33146, United States

Supporting Information

ABSTRACT: In this molecular docking study, the protonation states of the catalytic Asp dyad of the beta-secretase (BACE1) enzyme in the presence of eight chemically diverse inhibitors have been predicted. BACE1 catalyzes the rate-determining step in the generation of Alzheimer amyloid beta peptides and is widely considered as a promising therapeutic target. All the inhibitors were redocked into their corresponding X-ray structures using a combination of eight different protonation states of the Asp dyad for each inhibitor. Five inhibitors were primarily found to favor two different monoprotonated states, and the remaining three favor a dideprotonated state. In addition, five of them exhibited secondary preference for a diprotonated state. These results show that the knowledge of a single protonation state of the Asp dyad is not sufficient to search for the novel inhibitors of BACE1 and the most plausible state for each inhibitor must be determined prior to conducting in-silico screening.



1. INTRODUCTION

Alzheimer's disease (AD) is a neurological disorder that affects 5.1 million people in the United States alone.¹ AD is characterized by the deposition of extra cellular senile plaques inside the brain.^{2–4} The major components of these plaques are 40–42 amino acid residues containing peptides known as amyloid beta ($A\beta$) peptides.^{5–7} The $A\beta$ peptides are produced by the proteolytic cleavage of a trans membrane protein called amyloid precursor protein (APP) by two membrane bound aspartyl proteases namely, β -secretase (BACE1) and γ -secretase.^{3,8–10} BACE1 catalyzes the rate-limiting step of $A\beta$ generation by cleaving the Met671–Asp672 peptide bond of APP (isoform 770, identifier P05067) at the extracellular space.^{5,11,12} BACE1 knockout transgenic mice were shown to be unable to generate $A\beta$ from either endogenous APP¹³ or mutant APP transgene.¹⁴ These studies exhibited that the BACE1 knockout animals were normal in all other examined characteristics encouraging that anti-BACE1 therapy might target $A\beta$ production without major side effects. The inhibition of this enzyme can be used to titrate $A\beta$ down to levels that will not support the plaque formation associated with AD.^{5,11,12} However, BACE1 inhibitors with the appropriate pharmacokinetic and pharmacodynamic properties are currently elusive.^{15–17}

BACE1 constitutes a ubiquitous family of aspartyl proteases that is present in vertebrates, fungi, plants, and retroviruses.^{18–20} The N-terminal domain of the enzyme that is responsible for the catalytic activity exhibits 30% sequence identity to other members of this family such as pepsin, renin, and cathepsin D and possesses their common fold. In the quest

for novel inhibitors of BACE1, a large number of cocrystal structures (ca. 150) have been resolved with a variety of peptidic and nonpeptidic inhibitors bound to the ecto-domain of BACE1. These structures revealed that the active site of BACE1 contains a catalytic Asp dyad formed by two aspartate residues (Asp32 and Asp228).²¹ A wealth of experimental and theoretical data implicate the Asp dyad in the catalytic functioning of the entire family of aspartyl proteases.^{22–29} Site directed mutagenesis studies on BACE1 showed that the enzyme loses its activity upon mutation of either one of these aspartate residues.³⁰ In the general acid–base mechanism utilized by BACE1 Asp32 and Asp228 frequently alter their protonation states and function as an acid or base.^{23–25,29} The available crystal structures provide information regarding the interactions and bioactive conformations of the inhibitors at the active site. However, due to low resolution of these structures the protonation states of the Asp dyad cannot be determined in the presence of inhibitors. This information is required for the design of novel, specific, and blood brain barrier (BBB) permeable inhibitors of this enzyme. Therefore, the determination of the exact protonation states of these two Asp residues (Asp32 and Asp228) in the presence of specific inhibitors has become an area of intensive research.^{31–36}

As discussed below in most studies the protonation state of the Asp dyad has been investigated utilizing a hydroxyethylene (HE) based transition state inhibitor (OM99-2). In a classical molecular dynamics (MD) simulations and molecular docking

Received: December 19, 2011

Published: April 30, 2012



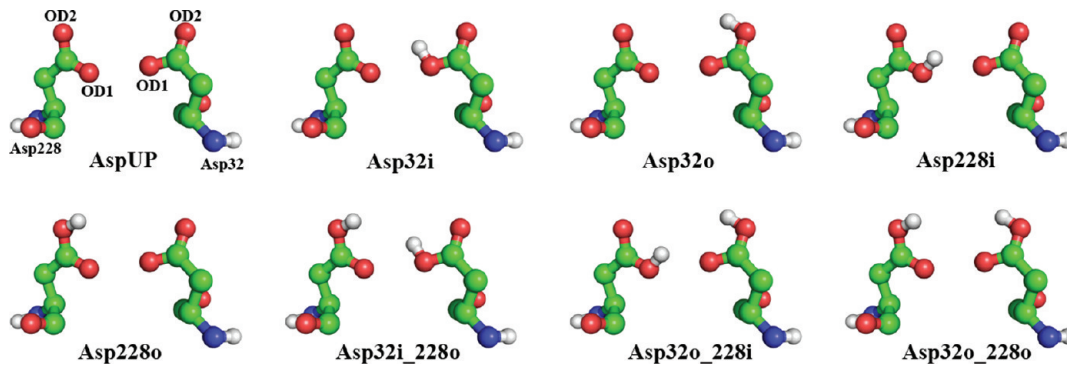


Figure 1. Possible protonation states of the catalytic Asp dyad (i = inner oxygen (OD1) and o = outer oxygen (OD2)).

Table 1. Chemical Structures, Experimental pHs, IC₅₀/K_i Values and PDB IDs of the Ligands

Ligands	Chemical Structure	Expt. pH	IC ₅₀ /K _i (nM)	PDB ID
L1 (HE)	A complex organic molecule containing a benzyl group, a carbamate group, and a cyclic amide.	6.5	1.1	2P4J ⁴⁸
L2 (AE)	A molecule with a central amine group linked to two phenyl groups via amide bonds.	NA	26	2FDP ⁴⁹
L3 (TC)	A molecule with a central sulfonamide group linked to two phenyl groups via amide bonds.	7.5	200	2IS0 ⁵⁰
L4 (CA)	A molecule with a central amine group linked to two phenyl groups via amide bonds.	NA	3	2QMF ⁵¹
L5 (RA)	A molecule with a central sulfonamide group linked to two phenyl groups via amide bonds.	7.5	8	2QZL ⁵²
L6 (AK)	A molecule with a central amine group linked to two phenyl groups via amide bonds.	NA	13	2WF4 ⁵³
L7 (ABP)	A molecule with a central amine group linked to two phenyl groups via amide bonds.	5.0	170000	2ZJM ⁵⁴
L8 (AP)	A molecule with a central amine group linked to two phenyl groups via amide bonds.	6.0	2000000	3HVG ⁵⁵

study, Park and Lee reported that a monoprotonated state in which the inner oxygen atom of Asp32 is protonated (Asp32i) is energetically more favorable than Asp228i for the HE inhibitor (inner (i) and outer (o) represent the OD1 and OD2 atoms of the carboxylate group of Asp respectively (Figure 1)).³³ The application of the linear scaling quantum method predicted the Asp228i and Asp32o_Aspx228i states at a high and low pH respectively in the presence of the same inhibitor.³⁴

atoms of the carboxylate group of Asp respectively (Figure 1)).³³ The application of the linear scaling quantum method predicted the Asp228i and Asp32o_Aspx228i states at a high and low pH respectively in the presence of the same inhibitor.³⁴

Merz et al. employed a QM/MM refinement technique on the eight different protonation states and suggested Asp32i as the most likely state in the presence of this inhibitor.³⁵ A recent study using the titration behavior of the Asp dyad supports a monoprotonated state that favors the protonation of Asp32 over Asp228 at a high pH and a diprotonated state at a low pH.³⁶ The molecular mechanics based binding affinity predictions on a set of HE based inhibitors also propose a neutral diprotonated Asp dyad as the most probable state.³⁷ In addition, Sussman et al. showed that in the presence of hydroxethylamine (HEA) based inhibitor the monoprotonated state is plausible at both low and high pH.³⁶ However, in the same study an amino group containing inhibitor was reported to prefer a dideprotonated Asp dyad at a high pH and a monoprotonated state at a low pH.³⁶ Furthermore, based on the titration curve and pK_a calculations, Polgár and Keserü suggested Asp32i as the most suitable protonation state for virtual screening.³⁸

All these studies explicitly showed that the chemical nature of the inhibitor played a key role in determining the protonation state of the Asp dyad. Several studies on other members of the aspartyl protease family such as HIV protease, endothiapepsin and renin also reported distinct protonation states of the Asp dyad in the presence of different inhibitors.^{39–44} Despite the availability of the wealth of experimental and theoretical data, there is no systematic study to predict the protonation states of the Asp dyad in the cocrystal structures of a wide range of chemically diverse inhibitors.

In the present study, this outstanding issue has been addressed through the application of molecular docking approach on eight inhibitors with distinct chemical scaffolds. In particular, (1) a hydroxyethylene (HE) based inhibitor (L1), (2) an aminoethyl (AE) based inhibitor (L2), (3) a tertiary carbinamine (TC) based inhibitor (L3), (4) a cyclic amine (CA) based inhibitor (L4), (5) a reduced amide (RA) based inhibitor (L5), (6) a hydrated α -amino keto (AK) group based inhibitor (L6), (7) an aminobenzylpiperidine (ABP) based inhibitor (L7), and (8) an aminopyrimidine (AP) based inhibitor (L8) were chosen to encompass large chemical diversity (Table 1). All eight possible protonation states (AspUP, Asp32i, Asp32o, Asp228i, Asp228o, Asp32i_228o, Asp32o_228i, and Asp32o_228o in Figure 1) of the Asp dyad for each inhibitor were considered. The inhibitors were then redocked to the corresponding crystal structures. The protonation states of the Asp dyad that provided the root-mean-square deviation (rmsd) below 2.0 Å from the crystallographic pose were considered for further analysis. In the literature the rmsd of a docking pose under this limit is generally considered to be a good reproduction of the crystal pose.^{45–47} The protonation state(s) of the Asp dyad in the presence of each inhibitor predicted by these docking trials were validated using the available experimental and theoretical data. The results reported in this study will advance our understanding of the influence of the distinct chemical environments of the inhibitors on the protonation states of the Asp dyad and help in the development of new virtual screening protocols to design novel BACE1 inhibitors.

2. COMPUTATIONAL METHOD

2a. Receptor Modeling. All the cocrystal structures of BACE1 with the following PDB IDs were taken from the PDB database: 2P4J,⁴⁸ 2FDP,⁴⁸ 2IS0,⁵⁰ 2QMF,⁵¹ 2QZL,⁵² 2WF4,⁵³ 2ZJM,⁵⁴ and 3HVG.⁵⁵ Only chain A of the crystal complex was

considered if the structure contains more than one crystal unit. The ligand–receptor complexes were then superposed to each other. In the next step, the ligand molecules were separated from the cocrystal complexes and hydrogen atoms were added to the amino acid residues of BACE1 using the YASARA program.⁵⁶ The eight different protonation states of Asp32 and Asp228 were assigned by keeping the OD1–CG–OD2–H or OD2–CG–OD1–H dihedral angle to 0°.

2b. Ligand Modeling. The eight different ligands selected for the docking trials adequately represent the chemical diversity of the functional groups that interact with the Asp dyad. These ligands were separated from their corresponding cocrystal structures for further processing. One of the most important factors in ligand–protein interactions is the proper protonation state of the ligand. In order to determine the protonation state of the ligand molecules, their pK_a values were computed at crystallographic pH using the Marvin program.⁵⁷ However, the crystallographic pH is not known for 3 out of 8 ligands (L2, L4, and L6 in Table 1). Based on the experimentally utilized pH range (5.0–7.5),^{48,50,54} the pK_a predictions for these three ligands were made at three different pH values (5, 6.5, and 7.5). It was observed that the predicted protonation states of all three ligands remain unchanged in this pH range.

2c. Molecular Docking. All molecular docking trials were performed using the AutoDock4.2 program.^{58,59} This is one of the most widely used docking engines and its scoring function for hydrogen bond directionality⁶⁰ is exploited in this study. The following multistep procedure was utilized for the docking of each ligand (inhibitor) to a different protonation state of the receptor (enzyme) using the Auto Dock tools (ADT):⁶¹ (i) The nonpolar hydrogens were merged and only the polar hydrogens were considered. (ii) The Gasteiger charges were added to the receptors and ligands molecules. (iii) A box size of 58 × 80 × 54 Å³ with grid spacing of 0.375 Å was defined around the active site of BACE1 such that it included all the residues that are critical for the interaction with the inhibitor. (iv) The grid maps around the active site of each BACE1 receptor were generated by the probe atoms utilizing the Auto Grid program. Each grid point in the map represents the potential energy of a probe atom in the presence of all the atoms of the receptor molecule. (v) The individual ligand molecules were docked at the active site of BACE1 in eight different protonation states of the Asp32 and Asp228 residues (Figure 1). The Lamarckian Genetic Algorithm (LGA) was used for the docking calculation. One hundred runs with 25 000 000 (maximum) evaluations and 270 000 generations were used for the docking simulation. After comparing the binding modes of the best docked poses derived from each simulation with the corresponding cocrystal structure of a ligand, the poses with the root-mean-square-deviation (rmsd) below 2.0 Å from crystal poses were chosen for further analysis. The PROPKA^{62–65} server was used to predict the pK_a of the Asp dyad in the presence of the inhibitors.

The predictions made by the AutoDock program were further validated by performing the docking trials using the GLIDE 5.6 Extra precision (XP) program.^{66–68} The structures for the docking were prepared using the Protein Preparation wizard incorporated in Maestro 9.1. A separate grid box of dimension 15 Å³ was constructed for each of the eight protonation states of the receptors by including all the residues around the ligand. The default values of the van der Waals scaling factor (1.00) and charge cutoff (0.25) were used for the

generation of the grid. All the ligands were processed with the LigPrep 2.4 module. The ionization states of the individual ligands were calculated at their corresponding crystallographic pH, if available, unless a range of pH 5.0–7.5 was considered to generate the appropriate protonation states. The default settings were considered for the docking protocol. Finally, the best docked poses of each ligand with the lowest Glide scores were chosen for further analysis.

The accuracy of the AutoDock docking protocol was also tested by comparing the protonation state of another aspartyl protease called endothiapepsin (PDB ID: 2JJI)⁴⁴ predicted by this program with the one proposed by X-ray crystallography and neutron diffraction experiments. In the presence of the gem-diol intermediate based inhibitor, Asp219o was experimentally observed to be the protonation state of the Asp dyad. On the basis of the low rmsd and binding energy, the docking results also showed that this state is the most plausible protonation state. Among the eight different states, Asp219o exhibited the lowest rmsd (<2.0 Å) and bound with the lowest binding energy (-9.77 kcal/mol), Supporting Information Table S11. The rmsd values for all other protonation states were found to be significantly higher. These results indicate that this docking protocol can correctly predict the protonation states of aspartyl proteases.

3. RESULTS AND DISCUSSION

All eight ligands (L1–L8 in Table 1) are self-docked into the corresponding X-ray structures with eight different protonation states of the two Asp residues for each receptor (Figure 1). The overall rmsd of docked poses and deviations of the atoms of the ligands that interact with the Asp dyad from their crystal structures and binding energies of ligands have been used as parameters to predict most plausible protonation states. The states predicted using these three parameters are further validated utilizing the available theoretical and experimental data.

3a. Hydroxyethylene (HE) Based Inhibitor. In the crystal structure (PDB ID: 2P4J) of the hydroxyethylene (HE) based inhibitor (L1 in Table 1), the O26 atom of L1 is located 2.6 and 2.4 Å away from the OD2 (Asp228) and OD1 (Asp32) atoms, respectively (Supporting Information Figure S1a). In the presence of the L1 inhibitor, the pK_a values computed using the PROPKA server are 8.81 and 5.23 for Asp32 and Asp228 respectively (Table 2). The higher pK_a value of Asp32 indicates that at the experimental pH (pH = 6.5) it exists in a monoprotonated state, while Asp228 remains unprotonated. However, the removal of the ligand from the enzyme (ligand-free BACE1) increases the predicted pK_a values of both Asp32

and Asp228 by 1.31 and 1.41 units, respectively, i.e. 10.12 for Asp32 and 6.64 for Asp228. These pK_a values suggest that both Asp residues exist in the protonated form in the ligand-free enzyme but the exact protonation state remains unknown. The docking of this inhibitor into the all eight protonation states of the Asp dyad provide the rmsd values lower than 2.0 Å from the crystal pose for both monoprotonated Asp228 (Asp228i and Asp228o) and diprotonated Asp (Asp32o_228i and Asp32o_228o) states (Table 3). In the Asp228o and Asp32o_228o states, the critical atoms C7 (\geq 1.5 Å) and O26 (\geq 3.0 Å) of L1 that are adjacent to the Asp dyad exhibit significant deviations (Figure 2a). However, the atomic deviations of these atoms are much smaller in the remaining two states (Asp228i and Asp32o_228i). The interaction energies of the individual atoms (O26 and H27) of the hydroxyl group (O26–H27) of L1 are also similar in these two poses (Figure 3a). The hydroxyl group forms a hydrogen bond with the inner oxygen of Asp32 in both cases (Asp228i (Figure 4a) and Asp32o_228i (Supporting Information Figure S1b)). In comparison to Asp32o_228i (rmsd = 1.77 Å), L1 is docked with a much lower rmsd in Asp228i (0.45 Å). The computed binding energy in the latter (-17.33 kcal/mol) is also ~2.0 kcal/mol lower than the one in the former (-15.54 kcal/mol). In addition to Asp228i (rmsd = 0.77 Å), the Glide XP docking program provides Asp32i (rmsd = 0.76 Å) as the state with the lowest rmsd. Among these two states, both the binding energy (-16.15 kcal/mol) and atomic deviations of C7 and O26 were found to be lower for Asp32i using this program (Supporting Information Table S2 and Figure S2a).

All these results suggest that the Asp228i, Asp32i, and Asp32o_228i states are possible in the presence of the L1 inhibitor, but based on the lower overall rmsd, greater binding energy, and predictions by two different programs (AutoDock and Glide XP), Asp228i is the most likely state. The differences in rmsd and binding energy between this state and the potential protonation states (Asp32i_AsP228i, Asp32i_AsP228o, Asp32o_AsP228i, or Asp32o_AsP228o) in the ligand-free enzyme are approximately 1.8–6.2 kcal/mol and 1.3–2.5 Å, respectively. This protonation state has also been proposed for the other members of the aspartyl protease family for the binding of the HE type of inhibitors. Using a linear scaling quantum method, Rajamani et al. reported that Asp228i is the most favored protonation state at a high pH, but the diprotonated state (Asp32o_228i) is also possible at low pH.³⁴ A thermodynamics based study on renin by Tokarski et al. also suggested a monoprotonated Asp226o (corresponding to Asp228 in BACE1) as the most favorable protonation state.⁴³ In a recent study, a monoprotonated form of the Asp dyad at a high pH (pH = 7.4) and a diprotonated form at a low pH (6.0) was favored.³⁶ Furthermore, a MD simulation study on HIV protease proposed this state.⁴⁰ On the other hand, in two previous studies Asp32i was suggested to be the most favorable for the HE based inhibitors.^{33,35}

3b. Aminoethyl (AE) Based Inhibitor. In the aminoethyl (AE) functional group containing inhibitor (L2 in Table 1), the AE group interacts with the Asp dyad. In the cocrystal structure (PDB ID: 2FDP), the N17 atom of L2 is located 2.9 Å away from the OD1 oxygen of both Asp32 and Asp228, and 3.5 and 2.6 Å from the OD2 oxygen of Asp32 and Asp228, respectively (Supporting Information Figure S3a). The PROPKA calculations on the ligand bound crystal structure provide the pK_a values of 7.07 and 2.43 for Asp32 and Asp228, respectively (Table 2). These values suggest that both Asp32 and Asp228

Table 2. pK_a Values of the Asp32 and Asp228 Residues Computed Using the PROPKA Server

ligand	BACE1 with Ligands		Ligand free BACE1	
	Asp32	Asp228	Asp32	Asp228
L1	8.81	5.23	10.12	6.64
L2	7.07	2.43	10.19	5.69
L3	6.12	2.66	10.51	5.51
L4	6.86	2.88	9.51	6.13
L5	7.75	2.79	5.73	9.66
L6	6.05	2.07	7.78	4.57
L7	2.98	7.10	9.42	5.85
L8	2.44	7.17	5.68	9.04

Table 3. Estimated Binding Affinity ΔG (kcal/mol) of the Docked Ligands and rmsd (\AA) from the Crystal Structure^a

	Ligand 1		Ligand 2		Ligand 3		Ligand 4		Ligand 5		Ligand 6		Ligand 7		Ligand 8	
	ΔG	RMSD														
AspUP	-14.15	2.30	-15.87	0.70	-16.05	1.39	-13.45	1.69	-16.18	1.15	-15.61	0.88	-11.17	0.90	-6.76	0.57
Asp32i	-11.20	3.42	-14.29	1.87	-14.99	1.44	-7.61	3.88	-7.98	5.53	-15.87	0.88	-11.08	0.81	-6.43	0.56
Asp32o	-13.33	2.73	-10.92	4.63	-15.70	1.22	-10.09	3.75	-15.38	1.15	-15.12	0.30	-12.20	4.99	-6.66	0.57
Asp228i	-17.33	0.45	-15.22	1.46	-15.85	0.45	-12.83	3.50	-16.52	1.33	-16.12	0.30	-11.22	0.85	-6.49	0.57
Asp228o	-13.45	1.64	-9.54	5.90	-15.16	1.38	-7.85	5.13	-15.11	2.32	-15.37	0.58	-11.27	4.96	-6.25	0.63
Asp32i_228o	-11.08	2.94	-10.59	4.97	-11.94	4.47	-10.15	3.54	-16.51	2.26	-15.55	0.52	-10.67	4.48	-5.86	1.30
Asp32o_228i	-15.54	1.77	-14.65	1.68	-15.40	0.46	-14.09	1.54	-8.74	5.88	-15.73	0.85	-11.33	4.68	-6.38	0.56
Asp32o_228o	-12.38	1.92	-11.86	2.41	-10.62	4.35	-10.21	3.54	-14.41	1.24	-14.67	0.71	-10.70	4.37	-6.12	0.66

^aThe poses with rmsds below 2.0 \AA and their energies are shown in red color.

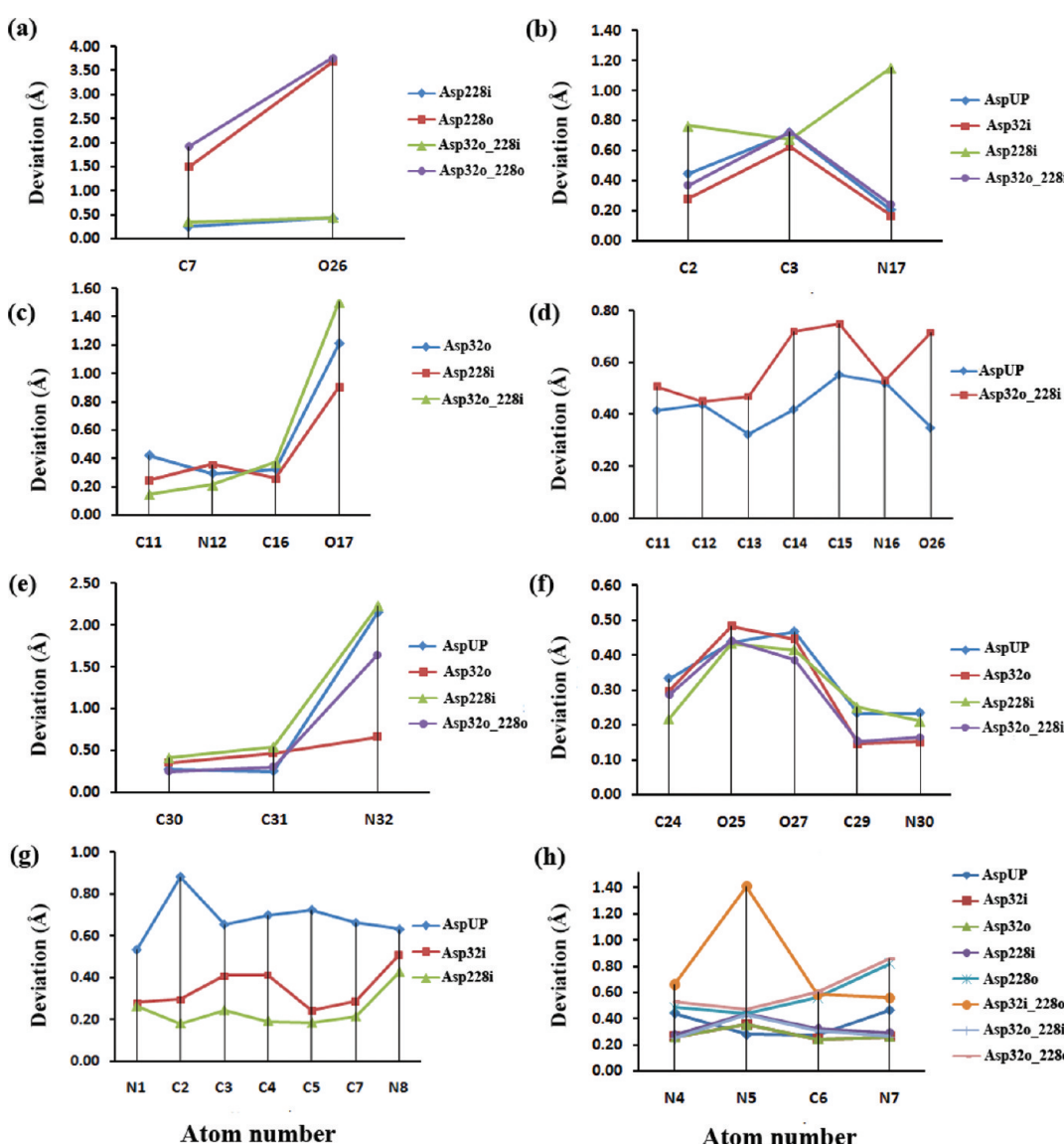


Figure 2. Atomic deviations (\AA) of critical atoms of the ligands in the docked pose. (a) Deviations of the C7 and O26 atoms of L1. (b) Deviations of the C2, C3, and N17 atoms of L2. (c) Deviations of the C11, N12, C16, and O17 atoms of L3. (d) Deviations of the C11, C12, C13, C14, C15, N16, and O26 atoms of L4. (e) Deviations of the C30, C31, and N32 atoms of L5. (f) Deviations of the C24, O25, O27, C29, and N30 atoms of L6. (g) Deviations of the N1, C2, C3, C4, C5, C7, and N8 atoms of L7. (h) Deviations of the N4, N5, C6, and N7 atoms of L8.

are unprotonated at a higher pH (pH = 7.4) and only Asp32 is protonated at a lower pH. However, in the ligand-free enzyme

the predicted pK_a values of both Asp32 and Asp228 are increased by 3.12 and 3.26 units respectively, i.e. 10.19 for

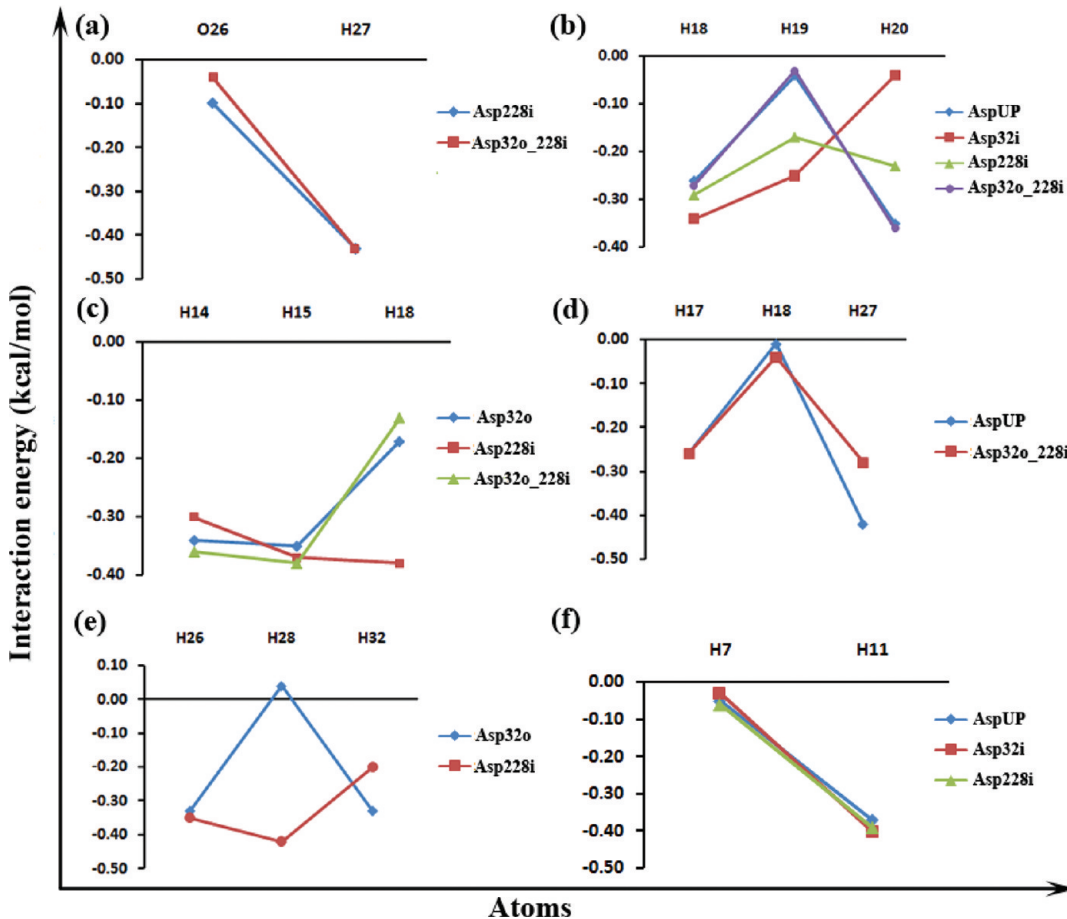


Figure 3. Interaction energies (kcal/mol) of the (a) O26 and H27 atoms from the hydroxyl group of L1; (b) H18, H19, and H20 atoms of the amide group of L2; (c) H14 and H15 atoms of the amide group and H18 of the hydroxyl group of L3; (d) H17 and H18 atoms of the amide group and H27 of the hydroxyl group of L4; (e) H26 and H28 atoms of the hydroxyl groups and H32 of the amine group of L6; (f) H7 and H11 atoms of the piperidine group of L7.

Asp32 and 5.69 for Asp228. This increase indicates that at a higher pH only Asp32 is protonated but at a lower pH both residues exist in a diprotonated form. The docking of L2 into its corresponding X-ray structure for all eight protonation states provided four states (AspUP, Asp32i, Asp228i, and Asp32o_Aspp228i) that exhibited rmsd under the cutoff value ($<2.0 \text{ \AA}$), Table 3. These states explicitly indicate that L2 does not prefer a state in which the outer oxygen atom of Asp228 is protonated i.e. Asp228o, Asp32i_228o, and Asp32o_228o. A closer scrutiny of the atoms (C2 and N17) of L2 that are close to the Asp dyad in all four potential states (AspUP, Asp32i, Asp228i, and Asp32o_Aspp228i) suggests that both atoms in Asp228i display higher atomic deviations than the ones in the remaining three states (Figure 2b). In this state, L2 loses its interactions with Arg128 (Supporting Information Figure S3b). In Asp32i, the interaction between the inhibitor and Thr232 is destroyed and the pose displays significantly higher rmsd (1.87 Å) than others (Supporting Information Figure S3c). However, in Asp32o_228i, L2 retains all the important interactions from the X-ray structure (Supporting Information Figure S3d). The interaction energies of atoms (H18, H19, and H20) of L2 that form hydrogen bonds with the Asp dyad provide another important parameter to predict the protonation state. The H18 atom interacts with the outer oxygen atom of Asp228 (Asp228o) and its interaction energy is quite similar in all four protonation states (Figure 3b). The H19 atom forms a

hydrogen bond with Gly230 and the lowest energy for its interaction was found in the Asp32i state. On the other hand, H20 forms a hydrogen bond with the inner oxygen atom of Asp32 (Asp32i) and exhibits strongest interaction in the AspUP and Asp32o_228i states (Figure 3b). Using the same parameters, the Glide XP program also suggests AspUP and another monoprotonated state, Asp32o, as the two most plausible states (Supporting Information Table S2 and Figure S2b).

A comparison of the overall rmsd and binding energies of L2 computed using the AutoDock and Glide XP programs suggest that AspUP, Asp32o_228i, and Asp32o as the probable states. The computed rmsd (0.70 Å in AspUP and 1.68 Å in Asp32o_228i) and binding energy (-15.87 kcal/mol in AspUP and -14.65 kcal/mol in Asp32o_228i) of these two states using AutoDock favor the AspUP state (Figure 4b). Since, in comparison to AspUP, the rmsd and binding energy of Asp32o_228i are only slightly higher (0.98 Å and 1.22 kcal/mol, respectively), this state is also possible. These two states are also supported by a recent study³⁶ in which L2 type of inhibitors were reported to favor the monoprotonated Asp dyad at a lower pH and the diprotonated Asp dyad at a higher pH (7.4). Both the atomic deviation of the N7 atom and binding energy computed using Glide XP also support the AspUP state, but the overall rmsd of Asp32o (0.61 Å) is slightly lower than AspUP (0.69 Å), Supporting Information Table S2

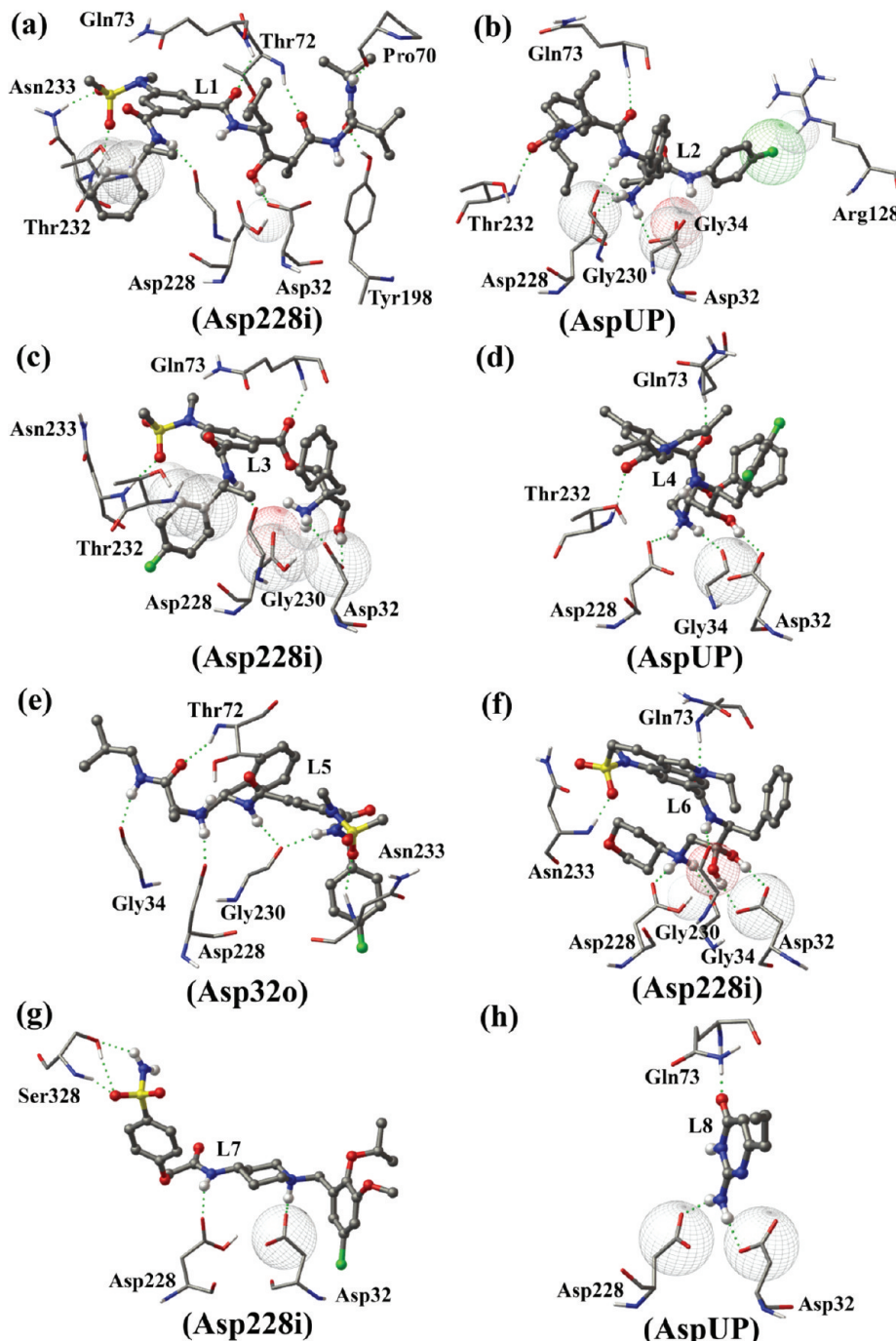


Figure 4. Most favorable binding poses of the ligands L1–L8 (a–h respectively). The dotted green lines and meshed spheres represent the hydrogen bond interactions and atomic close contacts respectively. Ball and sticks model represents the ligand and sticks represent the receptor.

and Figure S2b. All these results indicate that the AspUP state is the most likely state in the presence of L2 inhibitor. The differences in rmsd and binding energy between this state and the possible protonation states in the ligand-free enzyme at a low pH (Asp32i_228o, Asp32o_228o, or Asp32o_228i) are 0.9–4.2 Å and 1.2–5.3 kcal/mol respectively and at a high pH (Asp32i and Asp32o) are between 1.2–3.9 Å and 1.5–4.9 kcal/mol respectively.

3c. Tertiary Carbinamine (TC) Based Inhibitor. The tertiary carbinamine (TC) based inhibitor (L3) contains the HEA functional group that interacts with the Asp dyad of the enzyme (Table 1). In the cocrystal structure of this inhibitor

(PBD ID: 2IS0), the N12 atom of the amine group of L3 is positioned close to the OD1 and OD2 atoms of Asp32 and Asp228, respectively ($\text{N12}-\text{OD1}(\text{Asp32}) = 2.7 \text{ \AA}$ and $\text{N12}-\text{OD2}(\text{Asp228}) = 2.9 \text{ \AA}$ in Supporting Information Figure S4a). The O17 atom of L3 also located near the OD2 atom of Asp32 ($\text{N12}-\text{OD2}(\text{Asp32}) = 2.5 \text{ \AA}$). These geometrical parameters suggest that N12 is adjacent to the inner and outer oxygen atoms of the Asp32 and Asp228 residues respectively and O17 is close to the outer oxygen of Asp32. In this structure, the pK_a values computed using the PROPKA server are 6.12 and 2.66 for Asp32 and Asp228, respectively (Table 2). These values suggest that the dideprotonated state of the Asp dyad is likely

to be favored at the crystallographic pH (7.5). However, in the ligand-free BACE1, the pK_a values of both Asp32 and Asp228 are substantially increased by 4.39 and 3.25, respectively, i.e. Asp32 = 10.51 and Asp228 = 5.91. These values indicate that in the absence of L3, only Asp32 is protonated at the crystallographic pH. The docking of L3 into the eight different protonation states of the Asp dyad provided six docking poses (AspUP, Asp32i, Asp32o, Asp228i, Asp228o, and Asp32o_Aspx28i) that exhibit rmsd values lower than 2.0 Å from the crystal structure (Table 3). Among these states, in AspUP, Asp32i, and Asp228o, the critical N12 and O17 atoms of L3 display large atomic deviations from the crystallographic pose (>1.2 Å for N12 and >2.0 Å for O17 in Supporting Information Figure S4b). These deviations suggest the remaining three (Asp32o, Asp228i, and Asp32o_228i) as the potential protonation states. The N12 atom is quite stable and exhibits negligible displacements (<0.4 Å) in all three states (Figure 2c). However, the O17 atom in Asp32o and Asp32o_228i displays greater atomic displacements (>1.2 Å) than the one in Asp228i (Figure 2c). In the Asp228i state, the hydroxyl group of L3 makes a strong hydrogen bond with the outer oxygen of Asp32 (Figure 4c), while in Asp32o and Asp32o_228i it forms a weak hydrogen bond with the outer oxygen of Asp228 (Supporting Information Figure S4c and S4d). In Asp32o, one of the hydrogen bonds of L3 with the backbone (NH) of Gln73 is also broken (Supporting Information Figure S4c). Furthermore, in comparison to Asp32o and Asp32o_228i, in Asp228i the interaction energy of the H18 atom is the lowest (Figure 3c).

Comparisons of the overall rmsd (0.45 Å for Asp228i, 0.46 Å for Asp32o_228i, and 1.22 Å for Asp32o) and binding energy (-15.85 kcal/mol for Asp228i, -15.40 kcal/mol for Asp32o_228i, and -15.70 kcal/mol for Asp32o) between these states favor Asp228i. This type of monoprotonated state has also been previously proposed for the L3 type of inhibitors.³⁶ However, the Glide XP program provides Asp32o and AspUP as the two most likely states. Among them, both binding energy (-15.58 kcal/mol) and overall rmsd (0.39 Å) are lower for Asp32o but AspUP exhibits the lowest deviations of C11, N12, C16, and O17 atoms (Supporting Information Table S2 and Figure S2c). All these results suggest that a monoprotonated state (Asp228i or Asp32o) is the most likely state for this inhibitor. Among all eight inhibitors used in the present study, L3 is the only inhibitor for which the AutoDock and Glide XP programs suggest two different monoprotonated states. In this case, the determination of the protonation state will require more accurate quantum mechanics/molecular mechanics (QM/MM) methods. At the crystallographic pH, the ligand-free enzyme favors a monoprotonated form of Asp32 (Asp32i or Asp32o). The differences in rmsd and binding energy between the L3-bound and ligand-free enzyme are within a narrow range of 0.7–0.9 Å and 0.1–0.9 kcal/mol, respectively.

3d. Cyclic Amine (CA) Based Inhibitor. In the cocrystal structure (PDB ID: 2QMF) of the cyclic amine (CA) group containing HEA based inhibitor (L4 in Table 1), the N16 atom of the cyclic amine is positioned 2.6 Å away from the OD2 atom of Asp228. The O26 atom of the hydroxyl group of L4 is also located at a distance of 2.7 Å from the OD2 atom of Asp32 (Supporting Information Figure S5a). These geometrical parameters indicate that both N16 and O26 are located close to the outer oxygen of Asp228 and Asp32, respectively. The predicted pK_a values of 6.86 and 2.88 for Asp32 and Asp228,

respectively, indicate that a charged state of both Asp residues is favorable at a high pH (7.4) and monoprotonated Asp32 is favored at a low pH (pH < 6.0), Table 2. In the absence of L4, the pK_a values of Asp32 and Asp228 are increased by 2.65 and 3.25, respectively, i.e. Asp32 = 9.51 and Asp228 = 6.13. These pK_a shifts suggest that at a high pH only Asp32 is protonated, while at a low pH the Asp dyad is in a diprotonated state. The docking of L4 into eight different protonation states of the Asp dyad produces only two poses (AspUP and Asp32o_228i) that display rmsd values below 2.0 Å from the crystal structure (Table 3). In AspUP, the key atoms (C11, C12, C13, C14, C15, and O26) in the HEA moiety of L4 exhibit smaller atomic displacements than the ones observed in the Asp32o_228i case (Figure 2d). On the other hand, the positions of the C12 and N16 atoms remain unchanged in both these states. In AspUP, O26 of the hydroxyl group (O26–H27) forms a strong hydrogen bond with the outer oxygen of Asp32. However, in Asp32o_228i, this atom orients toward the inner oxygen of Asp32 and forms a hydrogen bond with it (Supporting Information Figure S5b). The interaction energy of the H27 atom (-0.43 kcal/mol) in AspUP is slightly lower than the one (-0.28 kcal/mol) in Asp32o_228i (Figure 3d). A comparison of binding energy (-14.09 kcal/mol for Asp32o_228i and -13.45 kcal/mol for AspUP) and overall rmsd (1.54 Å in Asp32o_228i and 1.69 Å in AspUP) indicates the preference of Asp32o_228i over AspUP. However, small atomic displacements of the key atoms of L4 near the Asp dyad favor the AspUP state (Figure 4d). The existence of this dideprotonated state is also supported by the PROPKA calculation at a high pH. Furthermore, on the basis of a low overall rmsd (0.74 Å) and the atomic deviations of the N16 and O26 atoms, this state is also predicted by the Glide XP program (Supporting Information Table S2 and Figure S2d).

All these results suggest that dideprotonated (AspUP) is the most favored state in the presence of the L4 inhibitor. The differences in rmsd and binding energy between this state and the possible protonation states in the ligand-free enzyme are 0.2–1.8 Å and 0.5–3.2 kcal/mol, respectively, at a low pH and 2.1–3.0 Å and 3.5–5.9 kcal/mol, respectively, at a high pH.

3e. Reduced Amide (RA) Based Inhibitor. In the cocrystal structure (PDB ID: 2QZL) of the reduced amide (RA) based inhibitor (L5 in Table 1), the N32 atom is located only 2.7 Å away from the OD2 of Asp228 (Supporting Information Figure S6a). In the presence of this inhibitor, the computed pK_a values of 7.75 and 2.29 for Asp32 and Asp228 respectively suggest a state in which only Asp32 is protonated at the crystallographic pH (7.5) (Table 2). The removal of L5 from the X-ray structure reduces pK_a of Asp32 by 2.02 and significantly increases this value by 6.87 unit for Asp228, i.e. Asp32 = 5.73 and Asp228 = 9.66. This is the largest shift in the pK_a value of Asp228 observed upon the binding of all the inhibitors (Table 2). These shifts in pK_a values suggest that at crystallographic pH the Asp32 and Asp228 exist in unprotonated and protonated forms respectively. Among the eight potential states, only four (AspUP, Asp32o, Asp228i, and Asp32o_228o) provide rmsds below 2.0 Å from the crystal structure (Table 3). An analysis of the atoms (C30, C31, and N32) of L5 that lie close to the Asp dyad reveals that the displacements of C30 and C31 are similar in all four states. The N32 atom provides the lowest deviation (0.6 Å) from the crystal pose for Asp32o and shifts more than 1.5 Å in the remaining three states (AspUP, Asp228i, and Asp32o_228o), Figure 2e. In AspUP, this atom moves away from Asp228 and

interacts with the backbone oxygen atom of Gly34 (Supporting Information Figure S6b). However, in Asp228i and Asp32o_228o, it also shifts away from Asp228 to interact with Asp32 (Supporting Information Figure S6c and S6d). A comparison of the binding energies of L5 in Asp228i (-16.52 kcal/mol), AspUP (-16.18 kcal/mol), Asp32o (-15.38 kcal/mol), and Asp32o_228o (-14.41 kcal/mol) shows a slight preference for the Asp228i state. On the other hand, both AspUP and Asp32o provide the lowest rmsds (1.15 Å) from the X-ray structure. On the basis of the PROPKA calculations, low fluctuation of the N32 atom and small difference in binding energy, among AspUP and Asp32o the later is slightly more favored (Figure 4e). However, an AspUP type of dideprotonated state has been proposed for HIV protease and renin.^{40,42} The docking results obtained from Glide XP also predicts Asp32o as the most plausible state. Among all eight states, this state provides the lowest overall rmsd (0.25 Å), the highest binding energy (-17.71 kcal/mol) and the smallest atomic deviation of the critical N32 atom (Supporting Information Table S2 and Figure S2e).

All these results indicate Asp32o as the most likely protonation state for the L5 inhibitor. At the crystallographic pH, the ligand-free enzyme supports a monoprotonated form of Asp228 (Asp228o or Asp228i). The differences between rmsd and binding energy in the L5-bound and ligand-free enzyme are within a narrow range of $0.3\text{--}1.1$ Å and $0.2\text{--}1.2$ kcal/mol, respectively.

3f. α -Amino Keto (AK) Based Inhibitor. The α -amino keto (AK) group containing inhibitor (L6 in Table 1) gets hydrated during the crystallization and mimics the gem-diol intermediate that is created during the mechanism. In the crystal structure of the L6 bound enzyme (PDB ID: 2WF4), the O25 and O27 atoms of the gem-diol group are located 2.9 and 2.5 Å away from OD1 and OD2 of Asp32, respectively, and N30 (L6) and OD2 (Asp228) are 2.8 Å apart from each other (Supporting Information Figure S7a). In the presence of this inhibitor, the pK_a values computed using the PROPKA server for Asp32 and Asp228 are 6.05 and 2.07 , respectively (Table 2). Since the crystallographic pH is not known, these values suggest that both Asp32 and Asp228 are likely to be deprotonated at a high pH (pH 7.5) and only former is protonated at a low pH (<6.0). In the ligand free enzyme, the predicted pK_a values of both Asp32 and Asp228 are increased by 1.73 and 2.50 respectively, i.e. Asp32 = 7.78 and Asp228 = 4.57 . These values indicate that both at a high and low pH Asp32 and Asp228 are in protonated and unprotonated forms respectively. Rather surprisingly, for the docking of L6 all poses exhibit rmsds below 1.0 Å (Table 3). However, the atomic displacements of atoms (C24, O25, O27, C29, and N30) of L6 that directly interact with the Asp dyad are under threshold limit for only four states (AspUP, Asp32o, Asp228i, and Asp32o_228i), Figure 2f. Since the displacements of these atoms for the remaining four states (Asp32i, Asp228o, Asp32i_228o, and Asp32o_228o) were comparatively higher (Supporting Information Figure S7b), they were not considered for further analysis. Among the four likely states (AspUP, Asp32o, Asp228i, and Asp32o_228i), Asp32o and Asp228i produced the best crystal poses (rmsd = 0.30 Å). Because these rmsd values are substantially lower than the ones in the other two cases (0.88 Å for AspUP and 0.85 Å for Asp32o_228i), only these two states are analyzed further. Although both Asp32o and Asp228i exhibit the same rmsd, their hydrogen bonding networks are significantly different. In

Asp32o, the amine ($-\text{NH}_2$) group of the inhibitor loses its hydrogen bond with Gly34, but this interaction remains intact in Asp228i (Supporting Information Figure S7c). Another important hydrogen bond is between the hydroxyl group (O27–H28) and the outer oxygen atom of Asp32. In Asp32o, this hydrogen bond is lost and the H28 atom orients in an upward direction to make an unfavorable interaction (Supporting Information Figure S7c). Due to these structural differences, in comparison to Asp32o, the interaction energy of H28 in Asp228i is lower (Figure 3e). The overall binding energy for Asp228i (-16.12 kcal/mol) is also 1.0 kcal/mol lower than the one in Asp32o (-15.12 kcal/mol). Glide XP also provides rmsd below 0.30 Å for the Asp32o (rmsd = 0.28 Å) and Asp228i (0.23 Å) states (Supporting Information Table S2). Although the binding energy for Asp32o (-14.55 kcal/mol) is higher than the one for Asp228i (-13.98 kcal/mol), the atomic deviations of the critical atoms O25, O27, and N30 are lower for Asp228i (Supporting Information Figure S2f).

On the basis of all these predictors, the Asp228i (Figure 4f) protonation state can be considered as the most plausible state in the presence of L6. A majority of theoretical and experimental studies regarding the reaction mechanism of BACE1 and HIV proteases suggest that the monoprotonated Asp is a required protonation state for stabilizing the gem-diol intermediate.^{22,24,25,29} A neutron diffraction study on endothiapepsin with a gem-diol intermediate containing inhibitor also shows that a monoprotonated state is the most favored protonation state.^{41,44} At both low and high pH, the ligand-free enzyme favors a monoprotonated form of Asp32 (Asp32o or Asp32i). The differences in rmsd and binding energy in the L6-bound and ligand-free enzyme are within a range of $0.0\text{--}0.5$ Å and $0.3\text{--}1.0$ kcal/mol, respectively.

3g. Aminobenzylpiperidine (ABP) Based Inhibitor.

The aminobenzylpiperidine (ABP) group containing inhibitor (L7 in Table 1) was discovered using the tethering technique.⁵⁴ In L7 bound cocrystal structure (PDB ID: 2ZJM), the N1 atom of the piperidine group and N8 of the amino group are positioned 3.0 Å and 2.8 Å away from OD2 of Asp32 and Asp228, respectively (Supporting Information Figure S8a). The predicted pK_a values of Asp32 and Asp228 from the PROPKA server indicate a low value for Asp32 (2.98) and high for Asp228 (7.10), Table 2. The experimental pH of 5.0 suggests that at this pH Asp32 and Asp228 are in charged and neutral states respectively. However, in the ligand-free enzyme the pK_a values of Asp32 and Asp228 are increased and decreased by 6.44 and 1.25 , respectively (Asp32 = 9.42 and Asp228 = 5.85). This is the largest increase observed in the pK_a value of Asp32 upon the binding of all the inhibitors (Table 2). These shifts in the pK_a values indicate that at the experimental pH both Asp32 and Asp228 exist in the protonated form. The predicted pK_a (6.97) of the N1 atom of piperidine group of L7 indicates that it is in the protonated state at this pH. The docking of L7 provides best poses only for the monoprotonated (Asp32i and Asp228i) and dideprotonated (AspUP) states of the Asp dyad (Table 3). These results suggest that the binding of L7 is favored only when the inner oxygen atom of either Asp residue is protonated or when both residues are unprotonated (AspUP). However, the binding of L7 is strongly disfavored when the outer oxygen of either Asp is protonated. Among the three potential states (Asp32i, Asp228i, and AspUP), the atoms (N1, C2, C3, C4, C5, C7, and N8) of L7 that lie near the Asp dyad show the smallest displacements in Asp228i (Figure 2g). However, the interaction energies of H7 and H11 are similar in

all three cases (Figure 3f). The “N1H7” group from the piperidine moiety and the amino (NH11) group attached to it form hydrogen bonds with the outer oxygen atoms of Asp32 and Asp228, respectively (Figure 4g and Supporting Information Figure S8b–c). The overall rmsd and binding energies of Asp32i, Asp228i, and AspUP are 0.81, 0.85, and 0.90 Å and –11.08, –11.22, and –11.17 kcal/mol, respectively. Glide XP provides the three lowest overall rmsd values for the AspUP (rmsd = 0.47 Å), Asp32i (rmsd = 0.63 Å), and Asp228i (rmsd = 0.64 Å) states (Supporting Information Table S2). Among them the highest binding energy (–9.40 kcal/mol) and the smallest deviations of critical atoms were observed for the Asp228i state (Supporting Information Table S2 and Figure S2g).

On the basis of the PROPKA calculations, overall rmsd, smaller fluctuations of critical atoms, and binding energies, Asp228i can be considered as the most likely protonation state in the presence of the L7 inhibitor. However, currently there is no experimental or theoretical data available to support this state. The differences in rmsd and binding energy between this state and a diprotonated state (Asp32i_Aspx228i, Asp32i_Aspx228o, Asp32o_Aspx228i, or Asp32o_Aspx228o) in the ligand-free enzyme are approximately 3.5–3.8 Å and 0.1–0.5 kcal/mol, respectively.

3h. Aminopyrimidine (AP) Based Inhibitor. The aminopyrimidine (AP) group containing inhibitor (L8 in Table 1) is the smallest among all the inhibitors considered in this study. In the cocrystal structure of this inhibitor (PDB ID: 3HVG), the N4 atom of L8 is located at a distance of 3.0 Å from the OD2 atom of Asp32 (Supporting Information Figure S9a). The N7 atom is 3.2 Å away from OD1 of Asp32 and 2.9 and 2.8 Å from the OD1 and OD2 atoms of Asp228, respectively. The predicted pK_a values by the PROPKA server for Asp32 and Asp228 are 2.44 and 7.17, respectively (Table 2). These values suggest that at an experimental pH of 6.0 the Asp dyad is monoprotonated and Asp228 and Asp32 exists in neutral and charged forms, respectively. In the ligand-free enzyme, the predicted pK_a values of both Asp32 and Asp228 are increased by 3.24 and 1.87, respectively, i.e. Asp32 = 5.68 and Asp228 = 9.04. These values indicate that at the experimental pH Asp32 and Asp228 are unprotonated and protonated, respectively. The computed pK_a of L8 suggests that the N4 atom is unprotonated at this pH. The docking of L8 provides seven poses that display rmsds below 1.0 Å from the crystal structure. The only exception is Asp32i_228o for which the rmsd is slightly higher (1.30 Å), Table 3. In all seven poses, the N4, N5, C6, and N7 atoms of L8 show very similar displacements (<1.0 Å) (Figure 2h). Among them, the five states (AspUP, Asp32i, Asp32o, Asp228i, and Asp32o_228i) display less than 0.60 Å deviation (Supporting Information Figure S9b–h). In these states, the interaction energies of the H10 and H11 hydrogen atoms are quite similar. The binding affinity for L8 follows the following pattern: AspUP (–6.76 kcal/mol) < Asp32o (–6.66 kcal/mol) < Asp228i (–6.49 kcal/mol) < Asp32i (–6.43 kcal/mol) < Asp32o_228i (–6.38 kcal/mol). The results obtained from AutoDock suggest that it is not trivial to predict the exact protonation state for this class of inhibitor. However, the Glide XP program provides the lowest rmsd (0.48 Å) and highest binding energy (–6.48 kcal/mol) for AspUP.

On the basis of the pK_a value, binding energy, rmsd, and atomic deviations, AspUP (Figure 4h) can be considered as the most favored protonation state for this class of inhibitors. There

are no relevant data available to support this protonation state in the presence of L8. At the crystallographic pH, the ligand-free enzyme supports a monoprotonated form of Asp228 (Asp228o or Asp228i). The differences in rmsd and binding energy between the L8-bound and ligand-free enzyme are within a narrow range of 0.2–0.5 Å and 0.0–0.1 kcal/mol, respectively.

4. CONCLUSIONS

In this molecular docking study, protonation states of the critical Asp dyad (Asp32 and Asp228) of BACE1 have been predicted in the presence of eight chemically diverse inhibitors. Eight structurally different scaffolds (HE, AE, TC, CA, RA, AK, ABP, and AP) of inhibitors are docked into the corresponding X-ray structure of BACE1 with eight potential protonation states of the Asp dyad (AspUP, Asp32i, Asp32o, Asp228i, Asp228o, Asp32i_228o, Asp32o_228i, and Asp32o_228o) for each inhibitor. The self-docking of these inhibitors using two different programs (AutoDock and Glide XP) showed that the mode of binding depends on the protonation state of the catalytic Asp dyad. The HE (L1), AK (L6), and ABP (L7) based inhibitors were found to prefer the monoprotonated Asp228i state. However, the L1 inhibitor also exhibits preference for the Asp32i state. The dideprotonated AspUP state is favored by the AE (L2), CA (L4), and AP (L8) inhibitors and RA (L5) prefers the monoprotonated Asp32o state. However, for the TC (L3) inhibitor, AutoDock and Glide XP programs predicted two different monoprotonated states (Asp228i and Asp32o). This is the only case in which it is not possible to predict the exact protonation state. The predicted binding energies of the most favored states show a good linear correlation (R^2 value of 0.79 and 0.75 for AutoDock and Glide XP respectively) with the calculated binding affinities (Figures 5 and Supporting Information S10). Moreover, the results

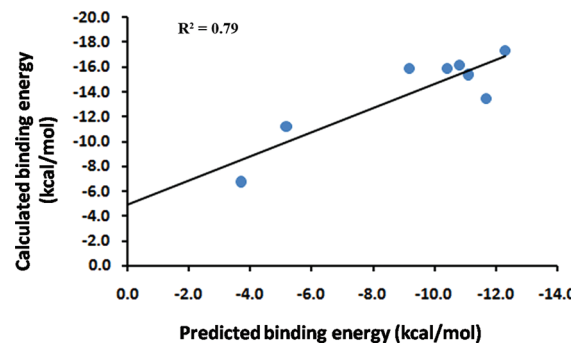


Figure 5. Linear regression analysis of the calculated binding energies (kcal/mol) by Auto Dock scoring function with the predicted binding energy (kcal/mol) from the reported inhibitory concentration values (nM).

reported in this study also show that multiple protonation states are possible for a single ligand. It is noteworthy that five out of eight ligands (L1, L2, L3, L4, and L5) show secondary preference for a diprotonated state. The possibility of multiple protonation states is also reported in a recent experimental and computational study by Dominguez et al.³⁶ They predicted large pK_a shifts (3.0–4.0 units) in the presence of different inhibitors.

The results presented in this study indicate that a single protonation state of the catalytic Asp dyad is not adequate to search for novel inhibitors of this critical enzyme through in-

silico screening. The most favored protonation states must be determined prior to conducting virtual screening. The protonation states predicted here need to be further refined using more accurate methods such as QM/MM and orthogonal space random walk (OSRW)⁶⁹ simulations with a large data set.

■ ASSOCIATED CONTENT

§ Supporting Information

Table S1–S2 and Figures S1–S10. This material is available free of charge via the Internet at <http://pubs.acs.org>.

■ AUTHOR INFORMATION

Corresponding Author

*E-mail: rpr@miami.edu. Tel.: 305-284-9372. Fax: 305-284-4571.

Notes

The authors declare no competing financial interest.

■ ACKNOWLEDGMENTS

A funding grant (DOH grant number 08KN-11) to R.P. from the James and Esther King Biomedical Research Program of the Florida State Health Department is acknowledged. We specially acknowledge Dr. Stephan Schürer for providing access to the Schrodinger suite program. Computational resources from the Center for Computational Science at the University of Miami are greatly appreciated. We thank Erica Sturm for her assistance in the preparation of the manuscript.

■ REFERENCES

- (1) Alzheimer's Disease Facts and Figures. *Alzheimer's & Dementia*; Alzheimer's Association, 2010; Vol. 6, p 6; www.alz.org.
- (2) Hardy, J.; Selkoe, D. J. The Amyloid Hypothesis of Alzheimer's Disease: Progress and Problems on the Road to Therapeutics. *Science* **2002**, *297*, 353–356.
- (3) Sipe, J. D. *Amyloid Proteins. The Beta Sheet Conformation and Disease*; WILEY-VCH Verlag GmbH & Co. KGaA: Weinheim, 2002; Vol. 2.
- (4) Hardy, J.; Allsop, D. Amyloid deposition as the central event in the aetiology of Alzheimer's disease. *Trends Pharmacol. Sci.* **1991**, *12*, 383–388.
- (5) Yan, R.; Bienkowski, M. J.; Shuck, M. E.; Miao, H.; Tory, M. C.; Pauley, A. M.; Brashler, J. R.; Stratman, N. C.; Mathews, W. R.; Buhl, A. E.; Carter, D. B.; Tomasselli, A. G.; Parodi, L. A.; Heinrikson, R. L.; Gurney, M. E. Membrane-anchored aspartyl protease with Alzheimer's disease [beta]-secretase activity. *Nature* **1999**, *402*, 533–537.
- (6) Pillot, T.; Drouet, B.; Queillé, S.; Labeur, C.; Vandekerckhove, J.; Rosseneu, M.; Pinçon-Raymond, M.; Chambaz, J. The Nonfibrillar Amyloid β -Peptide Induces Apoptotic Neuronal Cell Death. *J. Neurochem.* **1999**, *73*, 1626–1634.
- (7) Suo, Z.; Humphrey, J.; Kundtz, A.; Sethi, F.; Placzek, A.; Crawford, F.; Mullan, M. Soluble Alzheimers β -amyloid constricts the cerebral vasculature in vivo. *Neurosci. Lett.* **1998**, *257*, 77–80.
- (8) Vetrivel, K. S.; Barman, A.; Chen, Y.; Nguyen, P. D.; Wagner, S. L.; Prabhakar, R.; Thinakaran, G. Loss of Cleavage at β' -Site Contributes to Apparent Increase in β -Amyloid Peptide ($A\beta$) Secretion by β -Secretase (BACE1)-Glycosylphosphatidylinositol (GPI) Processing of Amyloid Precursor Protein. *J. Biol. Chem.* **2011**, *286*, 26166–26177.
- (9) Selkoe, D. J. Translating cell biology into therapeutic advances in Alzheimer's disease. *Nature* **1999**, *399*, A23–A31.
- (10) Thinakaran, G.; Koo, E. H. Amyloid Precursor Protein Trafficking, Processing, and Function. *J. Biol. Chem.* **2008**, *283*, 29615–29619.
- (11) Vassar, R.; Bennett, B. D.; Babu-Khan, S.; Kahn, S.; Mendiaz, E. A.; Denis, P.; Teplow, D. B.; Ross, S.; Amarante, P.; Loeloff, R.; Luo, Y.; Fisher, S.; Fuller, J.; Edenson, S.; Lile, J.; Jarosinski, M. A.; Biere, A. L.; Curran, E.; Burgess, T.; Louis, J.-C.; Collins, F.; Treanor, J.; Rogers, G.; Citron, M. β -Secretase Cleavage of Alzheimer's Amyloid Precursor Protein by the Transmembrane Aspartic Protease BACE. *Science* **1999**, *286*, 735–741.
- (12) Sinha, S.; Anderson, J. P.; Barbour, R.; Basi, G. S.; Caccavello, R.; Davis, D.; Doan, M.; Dovey, H. F.; Frigon, N.; Hong, J.; Jacobson-Croak, K.; Jewett, N.; Keim, P.; Knops, J.; Lieberburg, I.; Power, M.; Tan, H.; Tatsuno, G.; Tung, J.; Schenk, D.; Seubert, P.; Suomensari, S. M.; Wang, S.; Walker, D.; Zhao, J.; McConlogue, L.; John, V. Purification and cloning of amyloid precursor protein [beta]-secretase from human brain. *Nature* **1999**, *402*, 537–540.
- (13) Cai, H.; Wang, Y.; McCarthy, D.; Wen, H.; Borchelt, D. R.; Price, D. L. BACE1 is the major beta-secretase for generation of $A\beta$ peptides by neurons. *Nat. Neurosci.* **2001**, *4*, 233–234.
- (14) Luo, Y.; Bolon, B.; Kahn, S.; Bennett, B. D.; Babu-Khan, S.; Denis, P.; Fan, W.; Kha, H.; Zhang, J.; Gong, Y.; Martin, L.; Louis, J.-C.; Yan, Q.; Richards, W. G.; Martin Citron, M.; Vassar, R. Mice deficient in BACE1, the Alzheimer's β -secretase, have normal phenotype and abolished β -amyloid generation. *Nat. Neurosci.* **2001**, *4*, 231–232.
- (15) Martin, C. Emerging Alzheimer's disease therapies: inhibition of β -secretase. *Neurobiol. Aging* **2002**, *23*, 1017–1022.
- (16) Silvestri, R. Boom in the development of non-peptidic β -secretase (BACE1) inhibitors for the treatment of Alzheimer's disease. *Med. Res. Rev.* **2009**, *29*, 295–338.
- (17) May, P. C.; Dean, R. A.; Lowe, S. L.; Marten, F.; Sheehan, S. M.; Boggs, L. N.; Monk, S. A.; Mathes, B. M.; Mergott, D. J.; Watson, B. M.; Stout, S. L.; Timm, D. E.; Smith LaBell, E.; Gonzales, C. R.; Nakano, M.; Jhee, S. S.; Yen, M.; Ereshefsky, L.; Lindstrom, T. D.; Calligaro, D. O.; Cocke, P. J.; Greg Hall, D.; Friedrich, S.; Citron, M.; Audia, J. E. Robust Central Reduction of Amyloid- β in Humans with an Orally Available, Non-Peptidic β -Secretase Inhibitor. *J. Neurosci.* **2011**, *31*, 16507–16516.
- (18) Northrop, D. B. Follow the Protons: A Low-Barrier Hydrogen Bond Unifies the Mechanisms of the Aspartic Proteases. *Acc. Chem. Res.* **2001**, *34*, 790–797.
- (19) Davies, D. R. The Structure and Function of the Aspartic Proteinases. *Annu. Rev. Biophys. Biophys. Chem.* **1990**, *19*, 189–215.
- (20) Miller, M.; Jaskolski, M.; Rao, J. K. M.; Leis, J.; Wlodawer, A. Crystal structure of a retroviral protease proves relationship to aspartic protease family. *Nature* **1989**, *337*, 576–579.
- (21) Hong, L.; Koelsch, G.; Lin, X.; Wu, S.; Terzyan, S.; Ghosh, A. K.; Zhang, X. C.; Tang, J. Structure of the Protease Domain of Memapsin 2 (β -Secretase) Complexed with Inhibitor. *Science* **2000**, *290*, 150–153.
- (22) Chatfield, D. C.; Eurenus, K. P.; Brooks, B. R. HIV-1 protease cleavage mechanism: A theoretical investigation based on classical MD simulation and reaction path calculations using a hybrid QM/MM potential. *J. Mol. Struct.: THEOCHEM* **1998**, *423*, 79–92.
- (23) Suguna, K.; Padlan, E. A.; Smith, C. W.; Carlson, W. D.; Davies, D. R. Binding of a reduced peptide inhibitor to the aspartic proteinase from Rhizopus chinensis: implications for a mechanism of action. *Proc. Natl. Acad. Sci. U.S.A.* **1987**, *84*, 7009–7013.
- (24) Bjelic, S.; Åqvist, J. Catalysis and Linear Free Energy Relationships in Aspartic Proteases. *Biochemistry* **2006**, *45*, 7709–7723.
- (25) Cascella, M.; Micheletti, C.; Rothlisberger, U.; Carloni, P. Evolutionarily Conserved Functional Mechanics across Pepsin-like and Retroviral Aspartic Proteases. *J. Am. Chem. Soc.* **2005**, *127*, 3734–3742.
- (26) Piana, S.; Bucher, D.; Carloni, P.; Rothlisberger, U. Reaction Mechanism of HIV-1 Protease by Hybrid Car-Parrinello/Classical MD Simulations. *J. Phys. Chem. B* **2004**, *108*, 11139–11149.
- (27) Trylska, J.; Grochowski, P.; McCammon, J. A. The role of hydrogen bonding in the enzymatic reaction catalyzed by HIV-1 protease. *Protein Sci.* **2004**, *13*, 513–528.
- (28) Singh, R.; Barman, A.; Prabhakar, R. Computational Insights into Aspartyl Protease Activity of Presenilin 1 (PS1) Generating

- Alzheimer Amyloid β -Peptides ($A\beta40$ and $A\beta42$). *J. Phys. Chem. B* **2009**, *113*, 2990–2999.
- (29) Barman, A.; Schürer, S.; Prabhakar, R. Computational Modeling of Substrate Specificity and Catalysis of the β -Secretase (BACE1) Enzyme. *Biochemistry* **2011**, *50*, 4337–4349.
- (30) Hussain, I.; Powell, D.; Howlett, D. R.; Tew, D. G.; Meek, T. D.; Chapman, C.; Gloger, I. S.; Murphy, K. E.; Southan, C. D.; Ryan, D. M.; Smith, T. S.; Simmons, D. L.; Walsh, F. S.; Dingwall, C.; Christie, G. Identification of a Novel Aspartic Protease (Asp 2) as β -Secretase. *Mol. Cell. Neurosci.* **1999**, *14*, 419–427.
- (31) Cheng, Y.; Judd, T. C.; Bartberger, M. D.; Brown, J.; Chen, K.; Fremeau, R. T.; Hickman, D.; Hitchcock, S. A.; Jordan, B.; Li, V.; Lopez, P.; Louie, S. W.; Luo, Y.; Michelsen, K.; Nixey, T.; Powers, T. S.; Rattan, C.; Sickmier, E. A.; St. Jean, D. J.; Wahl, R. C.; Wen, P. H.; Wood, S. From Fragment Screening to In Vivo Efficacy: Optimization of a Series of 2-Aminoquinolines as Potent Inhibitors of Beta-Site Amyloid Precursor Protein Cleaving Enzyme 1 (BACE1). *J. Med. Chem.* **2011**, *54*, 5836–5857.
- (32) Ghosh, A. K.; Gemma, S.; Tang, J. β -Secretase as a therapeutic target for Alzheimer's disease. *Neurotherapeutics* **2008**, *5*, 399–408.
- (33) Park, H.; Lee, S. Determination of the Active Site Protonation State of β -Secretase from Molecular Dynamics Simulation and Docking Experiment: Implications for Structure-Based Inhibitor Design. *J. Am. Chem. Soc.* **2003**, *125*, 16416–16422.
- (34) Rajamani, R.; Reynolds, C. H. Modeling the Protonation States of the Catalytic Aspartates in β -Secretase. *J. Med. Chem.* **2004**, *47*, 5159–5166.
- (35) Yu, N.; Hayik, S. A.; Wang, B.; Liao, N.; Reynolds, C. H.; Merz, K. M. Assigning the Protonation States of the Key Aspartates in β -Secretase Using QM/MM X-ray Structure Refinement. *J. Chem. Theory Comput.* **2006**, *2*, 1057–1069.
- (36) Domínguez, J. L.; Christopeit, T.; Villaverde, M. C.; Gossas, T.; Otero, J. M.; Nyström, S.; Baraznenok, V.; Lindström, E.; Danielson, U. H.; Sussman, F. Effect of the Protonation State of the Titratable Residues on the Inhibitor Affinity to BACE-1. *Biochemistry* **2010**, *49*, 7255–7263.
- (37) Sussman, F.; Otero, J. M.; Villaverde, M. C.; Castro, M.; Domínguez, J. L.; González-Louro, L. L.; Estévez, R. J.; Estévez, J. C. On a Possible Neutral Charge State for the Catalytic Dyad in β -Secretase When Bound to Hydroxyethylene Transition State Analogue Inhibitors. *J. Med. Chem.* **2011**, *54*, 3081–3085.
- (38) Polgár, T.; Keserü, G. M. Virtual Screening for β -Secretase (BACE1) Inhibitors Reveals the Importance of Protonation States at Asp32 and Asp228. *J. Med. Chem.* **2005**, *48*, 3749–3755.
- (39) Yamazaki, T.; Nicholson, L. K.; Wingfield, P.; Stahl, S. J.; Kaufman, J. D.; Eymann, C. J.; Hodge, C. N.; Lam, P. Y. S.; Torchia, D. A. NMR and X-ray Evidence That the HIV Protease Catalytic Aspartyl Groups Are Protonated in the Complex Formed by the Protease and a Non-Peptide Cyclic Urea-Based Inhibitor. *J. Am. Chem. Soc.* **1994**, *116*, 10791–10792.
- (40) Harte, W. E.; Beveridge, D. L. Prediction of the protonation state of the active site aspartyl residues in HIV-1 protease-inhibitor complexes via molecular dynamics simulation. *J. Am. Chem. Soc.* **1999**, *121*, 3883–3886.
- (41) Coates, L.; Erskine, P.; Mall, S.; Gill, R.; Wood, S.; Myles, D.; Cooper, J. X-ray, neutron and NMR studies of the catalytic mechanism of aspartic proteinases. *Eur. Biophys. J.* **2006**, *35*, 559–566.
- (42) Hyland, L. J.; Tomaszek, T. A.; Meek, T. D. Human immunodeficiency virus-1 protease. 2. Use of pH rate studies and solvent kinetic isotope effects to elucidate details of chemical mechanism. *Biochemistry* **1991**, *30*, 8454–8463.
- (43) Tokarski, J. S.; Hopfinger, A. J. Constructing Protein Models for Ligand-Receptor Binding Thermodynamic Simulations: An Application to a Set of Peptidomimetic Renin Inhibitors. *J. Chem. Inf. Comput. Sci.* **1997**, *37*, 779–791.
- (44) Coates, L.; Tuan, H.-F.; Tomanicek, S.; Kovalevsky, A.; Mustyakimov, M.; Erskine, P.; Cooper, J. The Catalytic Mechanism of an Aspartic Proteinase Explored with Neutron and X-ray Diffraction. *J. Am. Chem. Soc.* **2008**, *130*, 7235–7237.
- (45) Waszkowycz, B.; Clark, D. E.; Gancia, E. Outstanding challenges in protein-ligand docking and structure-based virtual screening. *WIREs Comput. Mol. Sci.* **2011**, *1*, 229–259.
- (46) Österberg, F.; Morris, G. M.; Sanner, M. F.; Olson, A. J.; Goodsell, D. S. Automated docking to multiple target structures: Incorporation of protein mobility and structural water heterogeneity in AutoDock. *Proteins: Struct., Funct., Bioinf.* **2002**, *46*, 34–40.
- (47) Thilagavathi, R.; Mancera, R. L. Ligand-Protein Cross-Docking with Water Molecules. *J. Chem. Inf. Model.* **2010**, *50*, 415–421.
- (48) Ghosh, A. K.; Kumaragurubaran, N.; Hong, L.; Kulkarni, S. S.; Xu, X.; Chang, W.; Weerasena, V.; Turner, R.; Koelsch, G.; Bilcer, G.; Tang, J. Design, Synthesis, and X-ray Structure of Potent Memapsin 2 (β -Secretase) Inhibitors with Isophthalamide Derivatives as the P2-P3-Ligands. *J. Med. Chem.* **2007**, *50*, 2399–2407.
- (49) Yang, W.; Lu, W.; Lu, Y.; Zhong, M.; Sun, J.; Thomas, A. E.; Wilkinson, J. M.; Fucini, R. V.; Lam, M.; Randal, M.; Shi, X.-P.; Jacobs, J. W.; McDowell, R. S.; Gordon, E. M.; Ballinger, M. D. Aminoethylenes A Tetrahedral Intermediate Isostere Yielding Potent Inhibitors of the Aspartyl Protease BACE-1. *J. Med. Chem.* **2006**, *49*, 839–842.
- (50) Rajapakse, H. A.; Nantermet, P. G.; Selnick, H. G.; Munshi, S.; McGaughey, G. B.; Lindsley, S. R.; Young, M. B.; Lai, M.-T.; Espeseth, A. S.; Shi, X.-P.; Colussi, D.; Pietrak, B.; Crouthamel, M.-C.; Tugusheva, K.; Huang, Q.; Xu, M.; Simon, A. J.; Kuo, L.; Hazuda, D. J.; Graham, S.; Vacca, J. P. Discovery of Oxadiazoyl Tertiary Carbinamine Inhibitors of β -Secretase (BACE-1). *J. Med. Chem.* **2006**, *49*, 7270–7273.
- (51) Iserloh, U.; Wu, Y.; Cumming, J. N.; Pan, J.; Wang, L. Y.; Stamford, A. W.; Kennedy, M. E.; Kuvelkar, R.; Chen, X.; Parker, E. M.; Strickland, C.; Voigt, J. Potent pyrrolidine- and piperidine-based BACE-1 inhibitors. *Bioorg. Med. Chem. Lett.* **2008**, *18*, 414–417.
- (52) Coburn, C. A.; Stachel, S. J.; Jones, K. G.; Steele, T. G.; Rush, D. M.; DiMuzio, J.; Pietrak, B. L.; Lai, M.-T.; Huang, Q.; Lineberger, J.; Jin, L.; Munshi, S.; Katharine Holloway, M.; Espeseth, A.; Simon, A.; Hazuda, D.; Graham, S. L.; Vacca, J. P. BACE-1 inhibition by a series of $\psi[\text{CH}_2\text{NH}]$ reduced amide isosteres. *Bioorg. Med. Chem. Lett.* **2006**, *16*, 3635–3638.
- (53) Charrier, N.; Clarke, B.; Cutler, L.; Demont, E.; Dingwall, C.; Dunsdon, R.; Hawkins, J.; Howes, C.; Hubbard, J.; Hussain, I.; Maile, G.; Matico, R.; Mosley, J.; Naylor, A.; O'Brien, A.; Redshaw, S.; Rowland, P.; Soleil, V.; Smith, K. J.; Switzer, S.; Theobald, P.; Vesey, D.; Walter, D. S.; Wayne, G. Second generation of BACE-1 inhibitors part 3: Towards non hydroxyethylamine transition state mimetics. *Bioorg. Med. Chem. Lett.* **2009**, *19*, 3674–3678.
- (54) Yang, W.; Fucini, R. V.; Fahr, B. T.; Randal, M.; Lind, K. E.; Lam, M. B.; Lu, W.; Lu, Y.; Cary, D. R.; Romanowski, M. J.; Colussi, D.; Pietrak, B.; Allison, T. J.; Munshi, S. K.; Penny, D. M.; Pham, P.; Sun, J.; Thomas, A. E.; Wilkinson, J. M.; Jacobs, J. W.; McDowell, R. S.; Ballinger, M. D. Fragment-Based Discovery of Nonpeptidic BACE-1 Inhibitors Using Tethering. *Biochemistry* **2009**, *48*, 4488–4496.
- (55) Godemann, R.; Madden, J.; Krämer, J.; Smith, M.; Fritz, U.; Hesterkamp, T.; Barker, J.; Höppner, S.; Hallett, D.; Cesura, A.; Ebnet, A.; Kemp, J. Fragment-Based Discovery of BACE1 Inhibitors Using Functional Assays. *Biochemistry* **2009**, *48*, 10743–10751.
- (56) Krieger, E.; Vriend, G. Models@Home: distributed computing in bioinformatics using a screensaver based approach. *Bioinformatics* **2002**, *18*, 315–318.
- (57) Marvin view 5.5.0.1, 2011.05.12, ChemAxon (<http://www.chemaxon.com>).
- (58) Morris, G. M.; Goodsell, D. S.; Halliday, R. S.; Huey, R.; Hart, W. E.; Belew, R. K.; Olson, A. J. Automated docking using a Lamarckian genetic algorithm and an empirical binding free energy function. *J. Comput. Chem.* **1998**, *19*, 1639–1662.
- (59) Huey, R.; Morris, G. M.; Olson, A. J.; Goodsell, D. S. A semiempirical free energy force field with charge-based desolvation. *J. Comput. Chem.* **2007**, *28*, 1145–1152.

- (60) Huey, R.; Goodsell, D. S.; Morris, G. M.; Olson, A. J. Grid-Based Hydrogen Bond Potentials with Improved Directionality. *Lett. Drug Des. Discovery* **2004**, *1*, 178–183.
- (61) Sanner, M. F. Python: A Programming Language for Software Integration and Development. *J. Mol. Graphics Mod.* **1999**, *17*, 57–61.
- (62) Li, H.; Robertson, A. D.; Jensen, J. H. Very fast empirical prediction and rationalization of protein pKa values. *Proteins: Struct., Funct., Bioinf.* **2005**, *61*, 704–721.
- (63) Bas, D. C.; Rogers, D. M.; Jensen, J. H. Very fast prediction and rationalization of pKa values for protein–ligand complexes. *Proteins: Struct., Funct., Bioinf.* **2008**, *73*, 765–783.
- (64) Olsson, M. H. M.; Søndergaard, C. R.; Rostkowski, M.; Jensen, J. H. PROPKA3: Consistent Treatment of Internal and Surface Residues in Empirical pKa Predictions. *J. Chem. Theory Comput.* **2011**, *7*, 525–537.
- (65) Søndergaard, C. R.; Olsson, M. H. M.; Rostkowski, M.; Jensen, J. H. Improved Treatment of Ligands and Coupling Effects in Empirical Calculation and Rationalization of pKa Values. *J. Chem. Theory Comput.* **2011**, *7*, 2284–2295.
- (66) Friesner, R. A.; Banks, J. L.; Murphy, R. B.; Halgren, T. A.; Klicic, J. J.; Mainz, D. T.; Repasky, M. P.; Knoll, E. H.; Shelley, M.; Perry, J. K.; Shaw, D. E.; Francis, P.; Shenkin, P. S. Glide: A New Approach for Rapid, Accurate Docking and Scoring. 1. Method and Assessment of Docking Accuracy. *J. Med. Chem.* **2004**, *47*, 1739–1749.
- (67) Friesner, R. A.; Murphy, R. B.; Repasky, M. P.; Frye, L. L.; Greenwood, J. R.; Halgren, T. A.; Sanschagrin, P. C.; Mainz, D. T. Extra Precision Glide: Docking and Scoring Incorporating a Model of Hydrophobic Enclosure for Protein–Ligand Complexes. *J. Med. Chem.* **2006**, *49*, 6177–6196.
- (68) Halgren, T. A.; Murphy, R. B.; Friesner, R. A.; Beard, H. S.; Frye, L. L.; Pollard, W. T.; Banks, J. L. Glide: A New Approach for Rapid, Accurate Docking and Scoring. 2. Enrichment Factors in Database Screening. *J. Med. Chem.* **2004**, *47*, 1750–1759.
- (69) Zheng, L.; Chen, M.; Yang, W. Random walk in orthogonal space to achieve efficient free-energy simulation of complex systems. *Proc. Natl. Acad. Sci. U.S.A.* **2008**, *105*, 20227–20232.